

The phonon-assisted absorption of excitons in Cu_2O

Florian Schöne and Heinrich Stolz

Institut für Physik, Universität Rostock, Albert-Einstein-Strasse 23, D-18059 Rostock, Germany

Nobuko Naka

Department of Physics, Kyoto University, Kitshirakawa-Oiwake-cho, Sakyo-ku, Kyoto 606-8502, Japan

The basic theoretical foundation for the modelling of phonon-assisted absorption spectra in direct bandgap semiconductors, introduced by Elliott 60 years ago¹ using second order perturbation theory, results in a square root shaped dependency close to the absorption edge. A careful analysis of the experiments² reveals that for the yellow S excitons in Cu_2O the lineshape does not follow that square root dependence. The reexamination of the theory shows that the basic assumptions of constant matrix elements and constant energy denominators is invalid for semiconductors with dominant exciton effects like Cu_2O , where the phonon-assisted absorption proceeds via intermediate exciton states. The overlap between these and the final exciton states strongly determines the dependence of the absorption on the photon energy. To describe the experimental observed line shape of the indirect absorption of the yellow S exciton states we find it necessary to assume a momentum dependent deformation potential for the optical phonons.

PACS numbers: 71.35.Cc, 78.40.Fy, 63.20.kk, 71.35.-y

I. INTRODUCTION

The research focus in semiconductor physics has changed in recent decades from generic bulk semiconductors in favor for physical phenomena in more fancy systems, like lower dimensional structures. However, the discovery of yellow excitons with principal quantum numbers up to $n = 25$ ³ has renewed the interest of Cu_2O as it facilitates a novel branch of research in semiconductor physics⁴⁻⁹. These highly excited states, generally referred to as Rydberg excitons, exhibit similar properties already observed in atom physics but in a much more experimentalist friendly framework (effects such as Rydberg blockade are identifiable at liquid helium temperatures and the Stark effect manifests at rather low electric field strengths⁷). Furthermore, they additionally show new characteristics due to the unique setting within the semiconductor^{6,8,9}. The cubic symmetry of the system leads e.g. to anisotropic band dispersions, fine-structure splitting, or the breaking of antiunitary symmetries in magnetic fields¹⁰. Since the optical absorption bands of these Rydberg states sit on top of the phonon assisted absorption into the yellow exciton ground state, exhibiting a strong Fano-type interaction¹¹, a thorough understanding of the phonon-assisted absorption processes is of uttermost importance for properties of the Rydberg excitons.

The standard textbook approach to describe the shape of the phonon-assisted exciton absorption close to the band gap is based on second-order perturbation theory and goes back to Elliott¹. It can be visualized as a direct optical excitation into a dipole allowed virtual intermediate state and the subsequent relaxation to the final state through the emission of a phonon. Then by assuming the sum over the matrix elements and energy denominators to be constant, one can derive the well-known square root dependence of the absorption coefficient¹². In this paper,

we will critically examine these assumptions and show that in case of semiconductors with strong exciton effects, like Cu_2O , they are invalid mainly due to two reasons. First, the intermediate states are not pure band states, but also higher lying exciton states. Second, the assumptions that the deformation potential, which is used to describe the phonon interaction cannot be taken as a constant, but must be allowed to depend on the phonon wave vector \mathbf{Q} . Our theoretical analysis is strongly substantiated by experimental results, which indeed show not the expected square root behavior but the absorption coefficient rises more strongly at higher photon energies. A line shape fit of the absorption then allows to determine precise values for the deformation potential and its \mathbf{Q} -dependence. Since the green excitons are coming from the same valence band states as the yellow excitons, their absorption processes are closely connected. Therefore, we are able to describe the complete absorption band of the yellow and green series without additional parameters and obtain excellent agreement with experiment.

Our results also have practical interest for the use of Cu_2O in solar cells, as the absorption coefficient determines the cell efficiency. In a recent paper¹³, a detailed analysis of the whole absorption of Cu_2O up to the blue and violet exciton states was performed, but the authors used the simple square root dependence of the absorption coefficient and introduced ad hoc values for the deformation potentials for the green excitons to obtain a fit to the experimental spectrum, making their analysis invalid.

The paper is organized as follows: In the first section, we discuss the symmetry properties of Cu_2O relevant to the phonon-assisted absorption process. In the second paragraph the theoretical analysis is presented, while the next section discusses the experimental procedures. Then we discuss how to obtain the deformation potential from the fit of the theoretical expressions to the experimental results. In the last section, we extend the analysis to the

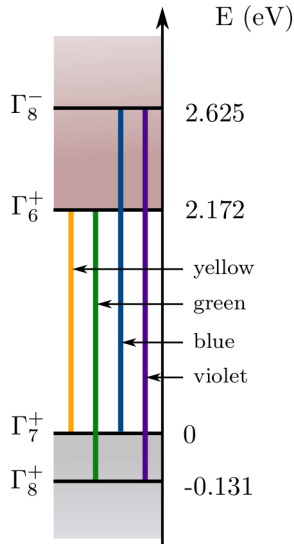


FIG. 1. The four exciton series in cuprous oxide with the respective band energies and symmetries at the Γ point.

green exciton states and discuss the results.

II. SYMMETRIES IN CUPROUS OXIDE

To comprehend the composition of effects contributing to the excitonic absorption spectra of cuprous oxide, we require some basic knowledge of its band structure.

The highest valence band stems from Cu $3d$ orbital with symmetry $\Gamma_3^+ \oplus \Gamma_5^+$ at the Γ point. Under the crystal field they split into the upper Γ_5^+ and lower Γ_3^+ bands. The Γ_5^+ bands splits via spin-orbit interaction further into a nondegenerate upper Γ_7^+ band and lower, twofold degenerate Γ_8^+ bands with a splitting of $\Delta_{so} = 131$ meV at zone center. The lowest conduction band originates from the Cu $4s$ orbital, hence possesses a Γ_1^+ symmetry and becomes a Γ_6^+ band under consideration of spin-orbit interaction. It is followed by a Γ_3^- band (Γ_8^- respectively, when including spin), that stems from the Cu $4p$ orbital, which is known from band structure calculations¹⁴. There are also higher located conduction bands with Γ_4^- symmetry that are formed by the Cu $4p$ orbital.

For our purposes, we are only interested in the two lowest conduction bands ($\Gamma_6^+ \oplus \Gamma_8^-$) and two highest valence bands ($\Gamma_7^+ \oplus \Gamma_8^+$), since they form the four known exciton series of cuprous oxide: the yellow ($\Gamma_6^+ \otimes \Gamma_7^+$), green ($\Gamma_6^+ \otimes \Gamma_8^+$), blue ($\Gamma_8^- \otimes \Gamma_7^+$) and violet ($\Gamma_8^- \otimes \Gamma_8^+$). They are visualised in Fig. 1.

Symmetries play an important role as they limit the possibilities for transition between the different bands. The symmetry of any respective exciton state is given by

$$\Gamma_{\text{exc}} = \Gamma_{\text{env}} \otimes \Gamma_{\text{c}} \otimes \Gamma_{\text{v}} \quad (1)$$

To enter any excitonic state directly, the exciton symmetry Γ_{exc} requires to coincide with the symmetry of the respective transition operator. In the O_h group the dipole operator \mathbf{p} possesses the symmetry Γ_4^- , the operator $(\mathbf{e} \cdot \mathbf{p})(\mathbf{k} \cdot \mathbf{r})$ yields the symmetry $\Gamma_3^+ \oplus \Gamma_4^+ \oplus \Gamma_5^+$, which corresponds to the electric quadrupole ($\Gamma_3^+ \oplus \Gamma_5^+$) and the magnetic dipole transitions (Γ_4^+). Regarding the excitonic envelope Γ_{env} , states with an S-like character bear Γ_1^+ symmetry, while P-like states show Γ_4^- symmetry. The yellow S excitons then split further into $\Gamma_1^+ \otimes (\Gamma_6^+ \otimes \Gamma_7^+) = \Gamma_2^+ \oplus \Gamma_5^+$ via exchange interaction. While the orthoexcitons (Γ_5^+) are at least quadrupole active, the paraexcitons (Γ_2^+) are inexcitable with light. The same relation holds true for the green S-excitions, which split as $\Gamma_1^+ \otimes (\Gamma_6^+ \otimes \Gamma_8^+) = \Gamma_3^+ \oplus \Gamma_4^+ \oplus \Gamma_5^+$. On the other hand the dipole transition to the higher located blue and violet S-states is possible as they decompose to $\Gamma_1^+ \otimes (\Gamma_8^- \otimes \Gamma_7^+) = \Gamma_3^- \oplus \Gamma_4^- \oplus \Gamma_5^-$ for blue and $\Gamma_1^+ \otimes (\Gamma_8^- \otimes \Gamma_8^+) = \Gamma_1^- \oplus \Gamma_2^- \oplus \Gamma_3^- \oplus 2\Gamma_4^- \oplus 2\Gamma_5^-$ for violet. For P-type excitons on the other hand, both the yellow $\Gamma_4^- \otimes (\Gamma_6^+ \otimes \Gamma_7^+) = \Gamma_2^- \oplus \Gamma_3^- \oplus \Gamma_4^- \oplus 2\Gamma_5^-$ and the green $\Gamma_4^- \otimes (\Gamma_6^+ \otimes \Gamma_8^+) = \Gamma_1^- \oplus \Gamma_2^- \oplus 2\Gamma_3^- \oplus 3\Gamma_4^- \oplus 3\Gamma_5^-$ series are dipole active. The beforementioned highly excited states up to $n = 25^3$ are the yellow series P excitons.

As we will see in the upcoming part, most of the absorption background superpositioning with the exciton resonances arises from the yellow S excitons. The prevalent contribution in the spectra, however, comes from the phonon-assisted absorption process. As mentioned, the dipole excitation from either the blue and violet S-excitions is possible. Treating the transition into the Γ_8^- band (or its respective exciton states) as a virtual state with a successive absorption or emission of a phonon, provided it has the correct symmetry, we are able to access the yellow (and green) S exciton states. Beyond the Γ_8^- conduction band, the next closest band that fulfills the necessary symmetry and parity restrictions to allow for a dipole transition into S-states would be a Γ_4^- valence band at around ~ -5 eV¹⁴. As we will see in the next paragraph, the strength of absorption contribution depends on the energy difference between the incoming light and the virtual state. Approximating the photon energy being around the yellow gap energy the ratio between the two dipole allowed states is $\left| \frac{\Delta E_{8^-,6^+}}{\Delta E_{4^-,7^+}} \right|^2 \simeq 0.01$, which however, might be compensated by a very strong electron-phonon interaction (as will be the case with the Γ_4^- phonon).

Cuprous oxide features 6 atoms in the primitive unit cell, hence there are 18 phonon branches¹⁵. The symmetry of the final exciton state must be contained in the direct product of the Γ_4^- and the corresponding phonon symmetry. Utilising multiplication tables of the O_h group¹⁶ it is easy to show that a Γ_5^+ exciton can couple to all odd parity phonons, while a Γ_4^+ state couples to all odd parity phonons except the Γ_2^- mode. Excitons with symmetry Γ_2^+ and Γ_3^+ only couple to Γ_5^- and Γ_4^- , Γ_5^- phonons, respectively. Additionally, to

enable a transition, phonon symmetry must also coincide with the predetermined transition symmetries of the bands, in the case of the second lowest conduction band $\Gamma_8^- \otimes \Gamma_6^+ = \Gamma_3^- \oplus \Gamma_4^- \oplus \Gamma_5^-$. From luminescence spectroscopy we know that the Γ_3^- optical phonon with an energy of $\hbar\omega_{3-} = 13.6$ meV at zone center is the dominant phonon branch. The contributions of all other phonons should be much weaker, except probably the Γ_4^- LO phonon at $\hbar\omega_{4-} = 82.1$ meV. Note that the coupling mechanism of all phonon modes is via the optical deformation potential, since Fröhlich interaction can only give rise to intraband transitions due to the orthonormality of the Bloch functions¹⁷. The even parity Γ_5^+ mode can in principle also contribute to the absorption by a wave vector dependent deformation potential, which has odd parity¹⁸.

III. THEORETICAL TREATMENT

Starting with the transition from excitonic vacuum to an exciton state μ with μ containing the set of quantum numbers (n, ℓ, m) of the final state, the transition probability can be derived by second order perturbation theory as

$$P_{0,\mu}(\mathbf{k}, \omega) = \frac{2\pi}{\hbar} \sum_{\mathbf{Q}, \lambda} \left| \sum_{\nu} \frac{\langle \Psi_{\mu, \mathbf{Q}+\mathbf{k}} | h_{\lambda, \mathbf{Q}} | \Psi_{\nu, \mathbf{k}} \rangle \langle \Psi_{\nu, \mathbf{k}} | h_{\text{ph}} | \Psi_0 \rangle}{E_{\nu}(\mathbf{k}) - \hbar\omega} \right|^2 \times \delta[E_{\mu}(\mathbf{Q} + \mathbf{k}) \mp \hbar\omega_{\lambda, \mathbf{Q}} - \hbar\omega], \quad (2)$$

for the absorption or emission of a phonon, respectively. The two transition elements consist of the electron-radiation interaction h_{ph} and the phonon interaction hamiltonians $h_{\lambda, \mathbf{Q}}$, with λ, \mathbf{Q} denoting the associated phonon type and its momentum. $E_i(\mathbf{k})$ represents the energy dispersion of state i , which is usually expressed in terms of the effective mass approximation $\frac{\hbar^2 k^2}{2M_i}$, with M_i being the respective excitonic mass.

We start by assuming the electron-radiation interaction in electric dipole approximation $h_{\text{ph}} = \frac{e}{m_0} \mathbf{A} \cdot \mathbf{p}$ since excitations over higher order processes (i.e. quadrupole excitation etc.) are negligibly small. As will be seen later, the main contribution to the phonon-assisted absorption stems from the 1S excitons of the yellow and green series, so we will restrict ourselves to final states with $\ell = 0$. Dipole transitions to states of the yellow and green series with S symmetry are forbidden, however this is not the case for the subsequent S series' of blue and violet excitons. The blue exciton series can be associated with the yellow series, since they share the same Γ_7^+ valence band, while the violet series share the Γ_8^+ valence bands with the green series. An excitation of $\ell = 1$ blue/violet excitons is inhibited by the negative parity of the P envelope, and higher order angular momenta are considered negligible. Our virtual states therefore consist solely of blue/violet S exciton states (depending on the final state being yellow or green respectively).

The experimental spectra are taken at a crystal temperature of around 2 K, where the occupation number of optical phonons converges to zero. Hence, we limit our examination to phonon emission. Furthermore, we consider the photon momentum \mathbf{k} to be negligibly small. The transition probability for the yellow excitons (as seen in Fig. 2) then takes the form

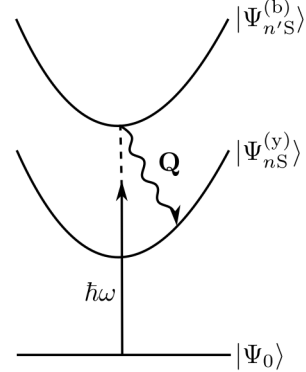


FIG. 2. A phenomenological depiction of the phonon-assisted transition as it is characterized by Eq. (4).

$$P_{0,nS}^{(y)}(\omega) = \sum_{\lambda} \bar{P}_{n,y}^{\lambda}(\omega) \quad (3)$$

$$\bar{P}_{n,y}^{\lambda}(\omega) = \frac{2\pi e^2}{\hbar m_0^2} \sum_{\mathbf{Q}} \times \left| \sum_{n'} \frac{\langle \Psi_{nS, \mathbf{Q}}^{(y)} | h_{\lambda, \mathbf{Q}} | \Psi_{n'S, 0}^{(b)} \rangle \langle \Psi_{n'S, 0}^{(b)} | \mathbf{A} \cdot \mathbf{p} | \Psi_0 \rangle}{E_{n'S}^{(b)}(0) - \hbar\omega} \right|^2 \times \delta[E_{nS}^{(y)}(\mathbf{Q}) + \hbar\omega_{\lambda, \mathbf{Q}} - \hbar\omega]. \quad (4)$$

The transition for the green series is equivalent to Eqs. (3), (4) by switching yellow to green ($y \rightarrow g$) and blue to violet ($b \rightarrow v$). For the sake of clarity though, we restrict the calculation to the yellow series. The phonon interaction matrix element in Eq. (4) can be rewritten in terms of the Bloch functions $\psi_{n, \mathbf{k}}$ of the associated bands as

$$\begin{aligned} \langle \Psi_{nS, \mathbf{Q}}^{(y)} | h_{\lambda, \mathbf{Q}} | \Psi_{n'S, 0}^{(b)} \rangle &= \\ &= \sum_{\mathbf{q}, \mathbf{q}'} \varphi_{nS, \mathbf{q}}^{(y)} \varphi_{n'S, \mathbf{q}'}^{(b)} \langle \psi_{6c, \frac{\mathbf{Q}}{2} + \mathbf{q}} | h_{3, \mathbf{Q}} | \psi_{8c, \mathbf{q}'} \rangle \\ &\quad \times \langle \psi_{7v, \frac{\mathbf{Q}}{2} - \mathbf{q}} | \psi_{7v, -\mathbf{q}'} \rangle \\ &= \sum_{\mathbf{q}} \varphi_{nS, \mathbf{q}}^{(y)} \varphi_{n'S, \mathbf{q} - \frac{\mathbf{Q}}{2}}^{(b)} \langle \psi_{6c, \frac{\mathbf{Q}}{2} + \mathbf{q}} | h_{3, \mathbf{Q}} | \psi_{8c, \mathbf{q} - \frac{\mathbf{Q}}{2}} \rangle. \end{aligned} \quad (5)$$

We are expanding the Bloch functions of the matrix elements in Eq. (5) around $\mathbf{q} = 0$ and express them via a

deformation potential $D_{\lambda;ij}$

$$\langle \psi_{6c, \frac{\Omega}{2}} | h_{\lambda, \mathbf{Q}} | \psi_{8c, \frac{\Omega}{2}} \rangle = D_{\lambda;68}(\mathbf{Q}) \sqrt{\frac{\hbar}{2\Omega\rho\omega_{\lambda}}}, \quad (6)$$

with Ω being the crystal volume, and ρ the density of Cu_2O . Consequently, the remainder of the sum reads as $\sum_{\mathbf{q}} \varphi_{n'S, \mathbf{q}}^{(y)} \varphi_{n'S, \mathbf{q}-\frac{\Omega}{2}}^{(b)}$. We assume $\varphi_{n'S, \mathbf{q}}^{(i)}$ to be hydrogen like envelope functions in momentum space. The sum can be evaluated by either simply inserting the momentum hydrogen wave functions¹⁹, or treating the expression as a convolution and integrate their product in position space. These convolution functions between different excitonic envelopes are known in the theory of phonon scattering as overlap functions¹¹. In our case of S type envelopes the spherical harmonics only introduce a factor of $1/(4\pi)$, which in both cases leaves us with a single integral which can be evaluated analytically. For the latter approach we would get

$$\begin{aligned} \mathcal{S}_{n, n'}^{(y, b)}(Q) &= \sum_{\mathbf{q}} \varphi_{n'S, \mathbf{q}}^{(y)} \varphi_{n'S, \mathbf{q}-\frac{\Omega}{2}}^{(b)} \\ &= \frac{2}{Q} \int_0^{\infty} dr r R_{n'S}^{(y)}(r) R_{n'S}^{(b)}(r) \sin \frac{Qr}{2}, \end{aligned} \quad (7)$$

with $R_{n'S}^{(i)}$ being the modified radial hydrogen wave functions. For the dominant transition over 1S states we get

$$\mathcal{S}_{1,1}^{(y, b)}(Q) = \frac{2^7 \beta^{3/2} (1 + \beta)}{(4(1 + \beta)^2 + a_y^2 \beta^2 Q^2)^2}, \quad (8)$$

where $\beta = a_b/a_y$ and a_y, a_b are the excitonic Bohr radii of the yellow and blue series.

The electron dipole interaction matrix element corresponds to the textbook solution

$$\langle \Psi_{n'S, 0}^{(b)} | \mathbf{A} \cdot \mathbf{p} | \Psi_0 \rangle = A_0 \varphi_{n'S}^{(b)}(\mathbf{r}=0) p_{78}, \quad (9)$$

with the dipole transition element between Bloch states $p_{78} = \langle u_{8c, \mathbf{q}} | \mathbf{e} \cdot \mathbf{p} | u_{7v, \mathbf{q}} \rangle$, which is considered to not vary significantly over \mathbf{q} . $\varphi_{n'S}^{(b)}(\mathbf{r})$ is the hydrogen like S envelope function in position space. For $\mathbf{r} = 0$ it abides to $\varphi_{n'S}^{(b)}(\mathbf{r}=0) = (\pi (a_b n')^3)^{-1/2}$.

Inserting the Eq. (5) to (9) into Eq. (4) we arrive at

$$\begin{aligned} \bar{P}_{n, y}^{\lambda}(\omega) &= \frac{e^2 A_0^2}{\Omega m_0 \rho \omega_{\lambda} a_b^3} \frac{|p_{78}|^2}{m_0} \\ &\times \sum_{\mathbf{Q}} |D_{\lambda;68}(\mathbf{Q})|^2 \left| \sum_{n'} \frac{\mathcal{S}_{n, n'}^{(y, b)}(Q)}{n'^{3/2} (E_{n'S}^{(b)} - \hbar\omega)} \right|^2 \\ &\times \delta [E_{n'S}^{(y)}(\mathbf{Q}) + \hbar\omega_{\lambda, \mathbf{Q}} - \hbar\omega]. \end{aligned} \quad (10)$$

The absorption coefficient is defined as

$$\alpha_{n, y}^{\lambda}(\omega) = \frac{2\hbar}{\varepsilon_0 n_{RC} \omega A_0^2} \bar{P}_{n, y}^{\lambda}(\omega), \quad (11)$$

with n_R being the refractive index around the excitation energy. To simplify the calculation, we assume that both the deformation potential and the 1S exciton dispersion have spherical symmetry, any deviation can in principle be treated, but would make the following integration more complex. In addition, the phonons of interest are optical phonons with only marginally varying energy dispersions¹⁸, hence their energies ω_{λ} will be considered constant. Under these circumstances the sum in Eq. (10) can be evaluated. Thus we obtain

$$\begin{aligned} \alpha_{n, y}^{\lambda}(\omega) &= \frac{e^2}{\pi^2 \hbar \rho \varepsilon_0 n_{RC} a_b^3} \frac{M_y}{m_0} \frac{q_n^{\lambda}}{\omega \omega_{\lambda}} \\ &\times \frac{|p_{78}|^2}{m_0} |D_{\lambda;68}(q_n^{\lambda})|^2 \\ &\times \left| \sum_{n'} \frac{\mathcal{S}_{n, n'}^{(y, b)}(q_n^{\lambda})}{n'^{3/2} (E_{n'S}^{(b)} - \hbar\omega)} \right|^2 \Theta(q_n^{\lambda}), \end{aligned} \quad (12)$$

with

$$q_n^{\lambda}(\omega) = \sqrt{\frac{2M_y}{\hbar^2}} \sqrt{\hbar\omega - \hbar\omega_{\lambda} - E_{n'S}^{(y)}}. \quad (13)$$

The square root behaviour of the textbook solution is still recognisable and is embedded in $q_n^{\lambda}(\omega)$, though Eq. (12) shows additional photon energy dependencies, such as the convolution of wave functions and the momentum dependent deformation potential. Furthermore, it is not depending on the Bohr radius of the final state, the yellow exciton, but on that of the blue exciton. Therefore, the dependence on the quantum number n of the yellow states is solely in the overlap factors $\mathcal{S}_{n, n'}^{(y, b)}$.

IV. EXPERIMENTAL DATA

Two samples were prepared to obtain absorption spectra in different photon energy ranges²⁰. For the observation of yellow exciton series, a thin slab of natural crystal Cu_2O was cut, mechanically polished, and then surface treated by NH_4OH . The thickness was measured as $160 \mu\text{m}$ by a caliper. For the observation of green exciton series, a thinner sample was grown by the melt-growth method as described in². Cu_2O powder was sandwiched between two MgO plates of $500 \mu\text{m}$ thickness, and then heated up to 1523 K above the melting point of Cu_2O . A wedge-shaped Cu_2O film was formed between the substrates after cooling down to room temperature. The film thickness was measured by a stylus profiler after removal of the top substrate. At the point of measurement film thickness is $10 \mu\text{m}$.

Absorption spectra were taken with samples at 2 K , immersed in superfluid helium in a cryostat. The white light from a halogen lamp, transmitted through the sample, was measured by a Peltier-cooled CCD camera (Wright Instruments) equipped at the back of a 25 cm monochromator with a 1200 g/mm grating blazed at 500

nm (JASCO CT-25T). Estimation of the reflectivity of light at the sample and substrate surfaces was difficult. In calculating the absorption coefficients

$$\alpha = -\ln \left[\frac{I_t}{b I_0} \right] / d, \quad (14)$$

we adjusted the magnitudes of the reference light (by the factor of b) so that the transmission at 620 nm wavelength becomes unity.²¹ Here, I_t and I_0 represent light intensities with and without a sample in the optical path, d is sample thickness.

V. DEFORMATION POTENTIAL AND YELLOW 1S PHONON TRANSITION

Taking a look back at Eq. (12), while providing us with an analytical solution for the absorption of the phonon background, it still harbors two uncertainties: The strength and momentum dependency of the deformation potential $D_{\lambda,68}$. Fortunately the phonon-assisted absorption into the yellow 1S exciton via the Γ_3^- LO phonon features a wide and distinctive spectral shape. We will utilize this property to do a fit of Eq. (12) unto the spectral data. In consideration of which blue S states actually contribute to this absorption line, one can easily calculate the ratios:

$$\frac{\mathcal{S}_{1,2}^{(y,b)}}{2^{3/2} \mathcal{S}_{1,1}^{(y,b)}} \lesssim 12\%, \quad (15)$$

$$\frac{\mathcal{S}_{1,3}^{(y,b)}}{3^{3/2} \mathcal{S}_{1,1}^{(y,b)}} \lesssim 3.7\%. \quad (16)$$

Since already the blue 3S contribution is small, the inner sum in Eq. (12) over the intermediate states is run up to $n' = 3$, which should be sufficient to safely neglect the contribution from higher blue states. The deformation potential can be expanded with respect to the square of phonon momentum Q to

$$\begin{aligned} D_{\lambda,68}(Q) &= D_{\lambda,68}^{(0)} + D_{\lambda,68}^{(2)} Q^2 + \dots \\ &\simeq D_{\lambda,68}^{(0)} \left(1 + \bar{D}_{\lambda,68}^{(2)} Q^2 \right). \end{aligned} \quad (17)$$

While usually the deformation potential is assumed to be constant, we will show that in case of the Γ_3^- phonon this is not the case. In this paper we will consider the zeroth and first order of Eq. (17). Higher order terms only increase the number of variables to fit and do not improve the result noticeably. For comparison we also fit the standard approach derived by Elliott¹ of the form

$$\alpha_E^\lambda(\omega) \propto \sum_{n=1} \frac{1}{n^3} \sqrt{\hbar\omega - \hbar\omega_\lambda - E_{nS}^{(y)}}. \quad (18)$$

The result can be seen in Fig. 3. While the assumption

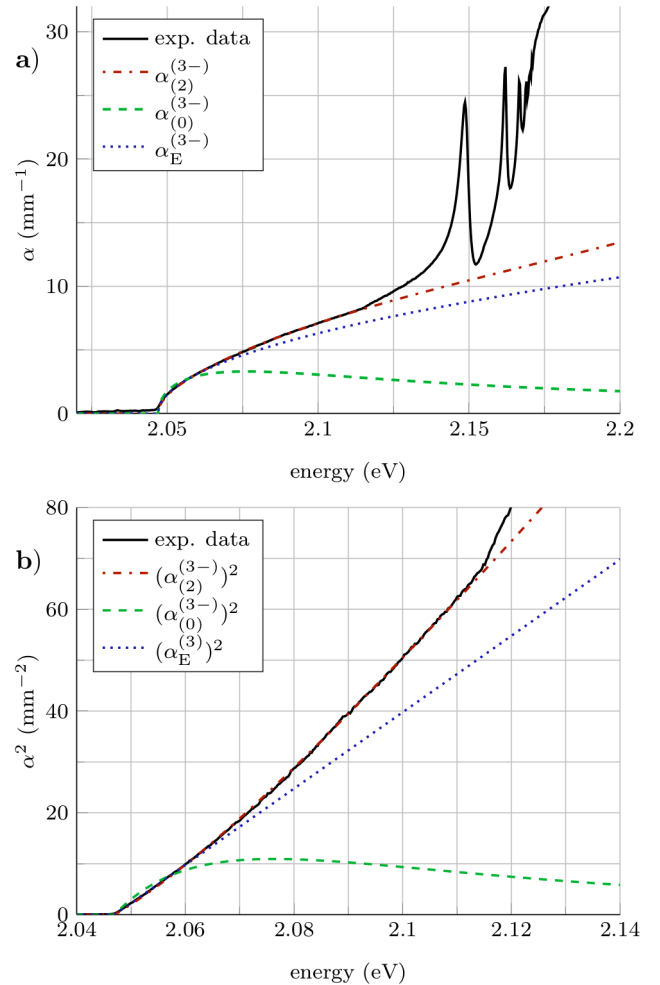


FIG. 3. Comparison of different fits for the absorption edge of the phonon-assisted 1S exciton for the sample of $160 \mu\text{m}$ thickness at 2K. While our theory flops for a constant deformation potential, the assertion of a momentum dependent deformation potential fits experimental data very well. In **b**) the absorption coefficient is squared for better visibility, clearly showing the non-square root behavior of the absorption coefficient for energies > 2.08 eV.

of a constant deformation potential $\alpha_{(0)}^{(3-)}$ fails to represent the experimental curve completely, the approach of Elliott $\alpha_E^{(3-)}$ fits well for a short energy range close to absorption edge, however deviates with increasing energy. The fit with the momentum dependent deformation potential $\alpha_{(2)}^{(3-)}$ reproduces the spectra neatly up to the start of the overlaying Γ_4^- phonon absorption edge, which can be seen as a shoulder around 2.116 eV at the upper right corner of Fig. 3 **b**).

The Γ_4^- phonon transition requires either Γ_4^- conduction or $\Gamma_2^- \oplus \Gamma_3^- \oplus \Gamma_4^- \oplus \Gamma_5^-$ valence bands²². While bands with these symmetries exist²³, we have to keep in mind, that they are located energetically quite far away from the yellow band gap E_g and we are not cognisant of any

Parameter	Value
density ²⁴	$\rho = 6.14 \times 10^3 \text{ kg/m}^3$
refractive index ²⁵	$n_R = 2.94$
1S exciton mass (y) ²⁵	$M_{1S}^{(y)} = 2.61 m_0$
Bohr radius (y) ²⁶	$a_y = 0.81 \text{ nm}$
Bohr radius (b)	$a_b = 1.72 \text{ nm}$
1S exciton energy (y) ²⁷	$E_{1S}^{(y)} = 2.033 \text{ eV}$
1S exciton energy (b) ²⁸	$E_{1S}^{(b)} = 2.569 \text{ eV}$
Γ_3^- phonon energy ¹⁸	$\hbar\omega_{3-} = 13.6 \text{ meV}$
Γ_4^- phonon energy ²⁹	$\hbar\omega_{4-} = 82.1 \text{ meV}$
dipole transition element	$ p_{78} ^2/m_0 = 2.66 \text{ eV}$

TABLE I. Necessary parameters to evaluate Eq. (12) for the transition into the yellow 1S state via the Γ_3^- phonon.

excitonic properties. Thus, the approach of Eq. (12) is not really suited for their treatment, and since the Γ_4^- phonon contribution is small enough, we purposely approximate it in the fashion of Eq. (18). The result of the fit is given in appendix A.

We stress, that all other phonons contribute with negligible strength to the yellow absorption band. The inclusion of the Γ_4^- phonon transition allows us to describe the phonon-assisted absorption into the 1S yellow exciton very accurately up to the P transitions.

The used parameters can be found in table I. The Bohr radius of the blue excitons is not explicitly known, thus for a systematic treatment they were calculated from the binding energies via $a_b = \text{Ry } a_B / (\text{Ry}_b \varepsilon_0)$, with Ry and a_B being the (hydrogen) Rydberg energy and Bohr radius, and $\varepsilon_0 = 7.5$ ³⁰. The dipole transition element can be obtained from experiments as well as $\mathbf{k} \cdot \mathbf{p}$ theory (see appendix B). The resulting fit parameters for the deformation potential of the Γ_3^- phonon-assisted absorption are

$$D_{3;68}^{(0)} = 25.45 \frac{\text{eV}}{\text{nm}}, \quad (19)$$

$$\bar{D}_{3;68}^{(2)} = 0.168 \text{ nm}^2. \quad (20)$$

The value for the static deformation potential $D_{3;68}^{(0)}$ is in well accordance to previous estimations³⁰.

VI. THE SPECTRUM BEYOND YELLOW 1S

A. Extrapolating the previous result

The practical aspect of the fitted parameters (19) and (20) is the fact that they are applicable for all Γ_3^- (and Γ_4^-) phonon-assisted transitions into the yellow S series, i.e. we additionally receive the absorption strengths for all $n \geq 2$ states. However, the contributions from states with $n > 2$ and into the yellow continuum, which would start at 2.186 eV, is negligible and will not be taken into account.

Another and perhaps more interesting proposition stems from the relation between transition elements of the yellow and green series. From group theoretical symmetry considerations it can be shown that

$$\frac{\alpha_{\text{g}}^{\Gamma_3^-}}{\alpha_{\text{y}}^{\Gamma_3^-}} = \frac{2}{1}. \quad (21)$$

The derivation is shown in appendix C. Therefore we also possess all necessary information to describe the Γ_3^- phonon-assisted transitions into the green S series. At zone center, symmetry considerations predict that the green series is supposed to consist of three distinct states Γ_3^+ , Γ_4^+ and Γ_5^+ . However, only the Γ_5^+ orthoexciton is accessible.

Beyond that, we consider the absorption into the yellow P exciton states phenomenologically to achieve a well-rounded depiction of the absorption spectrum. The excitonic resonances are accessed via a forbidden dipole transition¹, with the oscillator strength varying with principal quantum number as $(n^2 - 1)/n^5$. The line-shape of the P excitons can be described via asymmetric Lorentzians as derived by Toyozawa¹¹ and the successive transition into the yellow continuum is given by the Sommerfeld enhanced direct forbidden absorption¹². Recently, we have shown that the continuum absorption is shifted by an energy Δ_c into the P states due to plasma screening of charged residual impurities. In addition, the continuum absorption develops an Urbach tail behavior $\exp((\hbar\omega - E_g)/E_U)$ with E_U being the Urbach parameter³¹. These contributions are conglomerated into α_P , for details, see appendix A.

With the the fitted parameters in (19) and (20) we will now attempt to depict the absorption spectrum beyond the yellow band gap E_g . The total absorption coefficient only requires only the absorption channels that significantly participate and is therefore composed of

$$\alpha_{\text{tot}} = \alpha_{1,y}^{\Gamma_3^-} + \alpha_{2,y}^{\Gamma_3^-} + \alpha_{1,g}^{\Gamma_3^-} + \alpha_{1,y}^{\Gamma_4^-} + \alpha_{1,g}^{\Gamma_4^-} + \alpha_P. \quad (22)$$

The remaining parameters needed to evaluate α_{tot} are listed in table II. The green and violet Bohr radii are obtained in the same fashion, as it was done for the blue exciton. The yellow 2S exciton mass stems from the sum of effective electron and hole mass. Due to the almost equal binding energy of the yellow 1S paraexciton and the green 1S orthoexciton, and since they experience the same screening, it is expected that both masses are about equal. The result is shown in Fig. 4.

We recognise that the absorption spectrum is mainly constructed out of the Γ_3^- phonon-assisted transition of the yellow and green 1S exciton state, as well as the excitonic resonances and the absorption into the continuum at the band edge. While at an energy range around 2.2 eV the summed up absorption coefficient α_{tot} appears to slightly overestimate the absorption, beyond 2.22 eV the experimentally measured spectrum shows a steady increase in the absorption slope that is not reproduced in our theory.

Parameter	Value
2S exciton mass (y)	$M_{2S}^{(y)} = 1.56 m_0$
1S exciton mass (g)	$M_{1S}^{(g)} = 2.61 m_0$
Bohr radius (g)	$a_g = 0.74 \text{ nm}$
Bohr radius (v)	$a_v = 1.36 \text{ nm}$
2S exciton energy (y) ²⁷	$E_{2S}^{(y)} = 2.138 \text{ eV}$
1S exciton energy (g) ²⁷	$E_{1S}^{(g)} = 2.154 \text{ eV}$
1S exciton energy (v) ²⁸	$E_{1S}^{(v)} = 2.715 \text{ eV}$

TABLE II. Parameters to evaluate Eq. (22) for the remaining transitions, shown in Fig. 4.

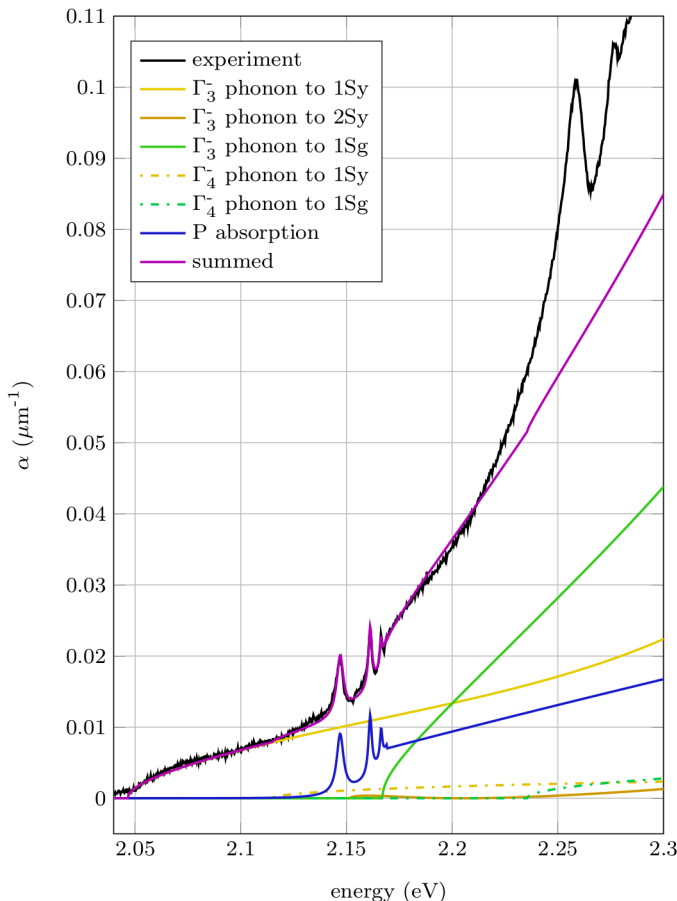


FIG. 4. The phonon-assisted absorption edge of the significantly contributing absorption participants α_{tot} . The sum of the individual participations is compared with the experimental spectrum of sample with thickness $10 \mu\text{m}$ at 2 K.

B. Discussion

We will first discuss the overshoot of the theoretical results over the experimental data at 2.2 eV.

The biggest issue in extrapolating the result of the yellow 1S exciton to the green 1S state is the fact that two of the essential exciton parameters are not explicitly known.

The excitonic Bohr radii used throughout this work are all extracted from the respective binding energies. They come into play via the overlap functions Eq. (8). The other parameters that determine the strength of the absorption are the exciton translational masses according to Eq. (13). Note that a change of 10% in the masses would alter the absorption by 15%. While for the 1S yellow state the mass has been determined experimentally to be $M_{1S_y} = 2.61 m_0$ ²⁵, for the 2S yellow and the green exciton series it is not known. However, for excitons with large principal quantum numbers, which are composed of valence and conduction band states near the zone center, the approximation $M_X = m_c + m_v$ holds true, where m_c and m_v are the effective masses at $k = 0$. Considering the effective mass of the conduction band $m_6 = 0.985 m_0$, and that of the Γ_7^+ hole of $m_7 = 0.575$, both from time-resolved cyclotron resonance³², we obtain for the 2S yellow exciton a mass of $1.56 m_0$.

For the green 1S state, whose wave function extends due to its large binding energy far into the Brillouin zone, the influence of the non-parabolicity of the Γ_8^+ valence bands on Bohr radius and effective mass are expected to be similar to that for the yellow 1S exciton. Using the heuristical relation between binding energy and translational mass as for the yellow state, we obtain a mass of $M_{1S_g} = 2.61 m_0$. The Bohr radius is given in table II. Of course, all these quantities are only first order approximations, and require extensive future work to improve. Theoretically, the Bohr radii and translational masses can be obtained from the solution of the \mathbf{K} -dependent effective mass equations, where \mathbf{K} is the center-of-mass wave vector, which will be the topic of a forthcoming paper. Experimentally, the masses can be obtained from resonance Raman studies involving the green P and the green 1S states, similar to that reported by Yu *et al.* in the 1970's²⁹ for the yellow exciton states. Here especially Raman processes involving acoustical phonons are of interest, since their Raman shift depends on their momentum, thus giving directly the dispersion of the green 1S states. These experiments would also clarify a possible contribution of a Γ_5^+ phonon to the absorption.

The most interesting finding of Fig. 4 is the steady increase of absorption in the region around 2.22 eV. This cannot be explained by simple modifications within this framework, i.e. the choice of parameters or of the wave function used. Theoretically, it could be explained by adding additional absorption channels, e.g. by introducing additional phonon interactions or exciton resonances, but it can easily be shown that this is not the case here. The only phonon resonance with a suitable energy to compensate the missing absorption would be the Γ_5^+ phonon at 63.8 meV. However, the possibility for a scattering into the green states involving the Γ_5^+ phonon can be ruled out, since the phonon possesses the wrong parity and such a process must also occur in comparable strength for the yellow 1S state but could not be identified in the analysis. The existence of a potential second green exciton series, that could be associated with the

Γ_8^+ light hole band dispersion, was considered, but since the Γ_8^+ valence bands are heavily coupled³³ no such additional exciton series should exist. Both ideas also seem implausible, since an additional phonon-assisted absorption edge would rise up abruptly in the spectrum, while the increase of the slope appears to be continuous.

Currently, the most logical explanation is a dependence of the excitonic parameters on exciton momentum \mathbf{K} . If the exciton mass is expected to steadily increase with exciton momentum, a smooth increase in phonon-assisted absorption with photon energy, as it is seen in the experiment, should be observed (cf. Eq. (13)). The same happens, if the green exciton Bohr radius increases, as the overlap functions (cf. Eq. 8) would also increase. A solution of this problem might come from the aforementioned study of the \mathbf{K} dependent effective mass equations.

Finally, we will discuss the topic of mixing between yellow and green exciton states, which was found in a recent study of the even excitons in Cu_2O ²⁶. According to this work, the lowest orthoexciton resonance (our 1S yellow state) is a mixture of yellow and green states with 7.2% green contribution. Taking this into account in our analysis would require the redetermination of the Deformation potential $D_{3,68}$ by refitting the Γ_3^- absorption band in the low energy part of the spectrum (cf. Fig. 3 b), but we expect only a small correction of the order of some percent due to the low green admixture. Much more pronounced should be the influence of mixing onto the absorption of the yellow “2s” and the green “1S” state. The former has more than 10% of green contributions, which would enhance its absorption strength considerably. In contrast, the green 1S state should have only a contribution of green states of about 40%, which, taking literally, should result in only half the absorption strength (cf. solid green line in Fig. 4). Both effects are clearly not consistent with the experimental data. However, a rigorous analysis would require the full wavefunctions of these exciton states, which is an interesting task for future work.

VII. CONCLUSION

In an effort to determine the phonon-assisted absorption background around the band edge of Cu_2O we evaluated the established second order perturbation treatment of Elliott. However, the resulting square root behaviour of this textbook solution is not sufficient to reliably reproduce experimentally measured spectra for energies much higher than the absorption edge. We reassessed the approach and removed three distinct approximations that are not necessarily justifiable. In a semiconductor with strong excitonic features, like Cu_2O , instead of treating intermediate states as pure band states we need to consider the corresponding exciton eigenstates for the virtual transition. Additionally, the momentum dependence of the optical phonons deformation potential was taken into account as well as the excitation energy depen-

dent denominator. The resulting improved expression of the absorption coefficient [Eq. (12)] is able to effectively model the Γ_3^- phonon-assisted transition into the yellow 1S exciton state, the strongest and most distinct phonon-assisted transition. Beyond that, we modelled the Γ_4^- phonon transition into the yellow 1S state and extrapolated our results from the yellow to the green series excitons. This yields a profound description of the phonon-assisted absorption background up to the yellow band gap. Beyond that, a sudden increase in the experimental absorption spectra is found, that could not be explained with our current theoretical treatment. The possibility of momentum dependent exciton parameters is discussed as a potential origin.

ACKNOWLEDGMENTS

We gratefully acknowledge support by the Collaborative Research Centre SFB 652/3 ‘Strong correlations in the radiation field’ funded by the Deutsche Forschungsgemeinschaft.

Appendix A: Fitting results for the minor absorption contributions

The Γ_4^- phonon transition:

As previously mentioned, the Γ_4^- phonon scattering is fitted with the square root solution of Eq. (18), as it couples to a multitude of higher (lower) located conduction (valence) bands, of which we cannot distinguish the individual transitions. Since its absolute contribution to the spectrum is marginal, we are content with only considering the $n = 1$ state. Utilising Eq. (13) we get

$$\alpha_{E^-}^{\Gamma_4^-}(\omega) = C_4 q_1^{\Gamma_4^-}(\omega), \quad (\text{A1})$$

with the corresponding fit parameter

$$C_4 = 6.56 \times 10^{-7}. \quad (\text{A2})$$

The yellow P-absorption:

The P-absorption is divided into three separate parts

$$\alpha_{\text{P}} = \alpha_{\text{Pcont}} + \alpha_{\text{Urbach}} + \sum_{n=2}^4 \alpha_{n\text{P}}. \quad (\text{A3})$$

The continuum is given by¹²

$$\alpha_{\text{Pcont}}(\omega) = C_{\text{yP}} \frac{(\hbar\omega - \tilde{E}_{\text{g}})^{3/2}}{\hbar\omega} \frac{\gamma e^{\gamma}}{\sinh \gamma} \left(1 + \frac{\gamma^2}{\pi^2}\right), \quad (\text{A4})$$

with

$$\gamma = \sqrt{\frac{\pi^2 R_{\text{y}}}{\hbar\omega - \tilde{E}_{\text{g}}}}, \quad (\text{A5})$$

and the yellow Rydberg energy⁹ $R_{y_y} = 87$ meV. The renormalized band gap $\tilde{E}_g = E_g + \Delta_c$ reflects the band gap shift due to plasma screening. Roughly, Δ_c can be estimated from the energy of the highest visible P exciton line ($n_{\max} = 4$) as $-87 \text{ meV}/n_{\max}^2$. It depends on the sample properties and thus is different for the thick and thin sample. The fit yields

$$C_{yP} = 9.82 \times 10^{-02} (\sqrt{eV} \mu\text{m})^{-1}. \quad (\text{A6})$$

The Urbach tail is given by

$$\alpha_{\text{Urbach}}(\omega) = C_U \exp\left(\frac{\hbar\omega - \tilde{E}_g}{E_U}\right) \theta(\tilde{E}_g - \hbar\omega), \quad (\text{A7})$$

with $C_U = 7.34 \times 10^{-03} \mu\text{m}^{-1}$ and $E_U = 9.8$ meV. The exciton resonances are described by asymmetric Lorentzians¹¹

$$\alpha_{nP}(\omega) = C_{nP} \frac{\Gamma_{nP}/2 + 2\xi_n \hbar(\omega - \omega_n)}{(\Gamma_{nP}/2)^2 + \hbar^2(\omega - \omega_n)^2}. \quad (\text{A8})$$

The values used are:

n	2P	3P	4P
$\hbar\omega_n^3$ (eV)	2.1472	2.1612	2.16604
C_{nP} ($10^{-5} \text{ eV}/\mu\text{m}$)	1.587	0.793	0.2645
Γ_{nP} (meV)	3.86	1.93	1.29
ξ_{nP} (10^{-3})	-4.32	-4.32	-4.32

Appendix B: Dipole transition element p_{78}

The dipole transition element of the blue exciton is related to the oscillator strength by

$$\frac{f_b}{\Omega_{uc}} = \frac{2}{\hbar\omega} \frac{|p_{78}|^2}{m_0} \left| \varphi_{1S}^{(b)}(0) \right|^2 = \frac{2}{\pi a_b^3} \frac{|p_{78}|^2}{\hbar\omega m_0}, \quad (\text{B1})$$

with $\Omega_{uc} = a_L^3$ being the volume of the uni cell, $a_L = 0.45$ nm is the lattice constant, and a_b is given in table I. In³⁴ the oscillator strength was determined to be $f_b = 1.2 \times 10^{-2}$. This yields for the dipole transition element

$$\frac{|p_{78}|^2}{m_0} = 2.726 \text{ eV}; \quad (\text{B2})$$

however this approach is reliant on the blue excitons Bohr radius, which is not well known. Therefore, we employ a second derivation to double check the result. The dipole transition element for the blue exciton series is related to the transition matrix element of the Γ_5^+ valence and Γ_3^- conduction band basis states by¹⁶

$$p_{78} = -\sqrt{\frac{2}{3}} \langle \varepsilon_3^+ | \mathbf{p} | \gamma_2^- \rangle. \quad (\text{B3})$$

The transition matrix element of Eq. (B3) appears in the Suzuki-Hensel Hamiltonian³⁵ in the coefficient

$$G = \frac{2}{m_0} \sum_{\ell=\Gamma_3^-} \frac{|\langle \varepsilon_3 | p_z | \gamma_2^-, \ell \rangle|^2}{E_{5v} - E_\ell}, \quad (\text{B4})$$

coupling all Γ_3^- bands to the respective Γ_5^+ band. The coupling coefficients are directly connected to the three dimensionless parameters A_i ($i = 1, 2, 3$) of the Hamiltonian. Albeit the dipole coupling to a Γ_5^+ band is possible via four different symmetries $\Gamma_4^- \otimes \Gamma_5^+ = \Gamma_2^- \oplus \Gamma_3^- \oplus \Gamma_4^- \oplus \Gamma_5^-$, and thus there should exist four separate coupling coefficients, band structure calculations of Cu_2O show²³, that no Γ_2^- band is located in the near vicinity of the Γ_5^+ valence band. Therefore when the coupling coefficient for Γ_2^- is neglected, the system of equations is solvable. The dimensionless parameters A_i are known from band structure fits⁹ and result in a value of

$$G = -2.973. \quad (\text{B5})$$

As there is also only one Γ_3^- band in the vicinity of the Γ_5^+ band, the coupling coefficient G can be associated with the matrix element in Eq. (B3), hence

$$\frac{|p_{78}|^2}{m_0} = 2.662 \text{ eV}. \quad (\text{B6})$$

Both results are in fairly good agreement. For the estimation of the static deformation potential, we use the result of Eq. (B6).

Appendix C: Phonon-assisted transition strength of the yellow and green series

We are denoting the band to band dipole transition matrix element between Γ_{5v}^+ and Γ_{3c}^- bands of Eq. (B3) as

$$p_{35} = \langle \varepsilon_3^+ | \mathbf{p} | \gamma_2^- \rangle. \quad (\text{C1})$$

We now calculate the relative strength of the dipole transition strength of the blue and violet transition, respectively. We are only interested in the Γ_4^- states, as they are the only ones accessible via the dipole operator \mathbf{p} . The composition of these states is known from the coupling coefficients of the O_h group¹⁶. The resulting dipole transition matrix elements read as

$$\langle 0 | \mathbf{p} | Z \rangle_b = -\sqrt{\frac{2}{3}} p_{35}, \quad (\text{C2})$$

$$\langle 0 | \mathbf{p} | Z \rangle_{v,1} = -\sqrt{\frac{6}{5}} p_{35}, \quad (\text{C3})$$

$$\langle 0 | \mathbf{p} | Z \rangle_{v,2} = -\sqrt{\frac{2}{15}} p_{35}, \quad (\text{C4})$$

For the phonon-assisted transition, we additionally need to consider the transition strength of the phonon process. The transition probability has the form

$$P_{0,\mu} \propto \sum_{\lambda} \left| \sum_{\nu} \langle \Psi_{\mu} | h_{\lambda} | \Psi_{\nu} \rangle \langle \Psi_{\nu} | \mathbf{p} | \Psi_0 \rangle \right|^2. \quad (\text{C5})$$

As we are primarily interested in the transition that is facilitated by the Γ_3^- phonon, we restrict the sum over λ to the constituents of this respective phonon branch. The Γ_3^- phonon can theoretically scatter into $\Gamma_4^- \otimes \Gamma_3^- = \Gamma_4^+ \oplus \Gamma_5^+$ states. For the yellow series only the Γ_5^+ ortho-exciton states contribute, the green series exhibits Γ_5^+ ortho- as well as Γ_4^+ para-exciton states. However, since the Γ_3^- phonon transition cannot inflict a change to the spin-configuration of the intermediate state, the scattering into Γ_4^+ states is not occurring. This can also readily be seen when the coupling strengths of the transitions are evaluated, where the Γ_4^+ participating states cancel each other out. The Γ_3^- phonon transition operator h_3 ³⁶ has two constituents, η_{31} and η_{32} . Their coupling between the Γ_8^- and Γ_6^+ conduction band can be expressed via

$$\eta_{31} \begin{pmatrix} |8c, -\frac{3}{2}\rangle \\ |8c, -\frac{1}{2}\rangle \\ |8c, +\frac{1}{2}\rangle \\ |8c, +\frac{3}{2}\rangle \end{pmatrix} = \frac{\tilde{D}_{3;68}}{\sqrt{2}} \begin{pmatrix} 0 \\ |6c, -\frac{1}{2}\rangle \\ -|6c, +\frac{1}{2}\rangle \\ 0 \end{pmatrix}, \quad (\text{C6})$$

$$\eta_{32} \begin{pmatrix} |8c, -\frac{3}{2}\rangle \\ |8c, -\frac{1}{2}\rangle \\ |8c, +\frac{1}{2}\rangle \\ |8c, +\frac{3}{2}\rangle \end{pmatrix} = \frac{\tilde{D}_{3;68}}{\sqrt{2}} \begin{pmatrix} -|6c, +\frac{1}{2}\rangle \\ 0 \\ 0 \\ |6c, -\frac{1}{2}\rangle \end{pmatrix}, \quad (\text{C7})$$

with $\tilde{D}_{\lambda,ij} = \hbar D_{\lambda,ij} / \sqrt{2\Omega\rho E_{\lambda}}$. The transformed intermediate Γ_4^- states receive the structure of their Γ_5^+ counterparts, and utilising the orthonormality of the exciton

states then eliminates coupling to most of the states. The phonon transition elements then read as follows

$${}_y\langle XY | \eta_{31} | Z \rangle_b = 0, \quad (\text{C8})$$

$${}_y\langle XY | \eta_{32} | Z \rangle_b = -\frac{\tilde{D}_{3;68}}{\sqrt{2}}, \quad (\text{C9})$$

$${}_g\langle XY | \eta_{31} | Z \rangle_{v_1} = 0, \quad (\text{C10})$$

$${}_g\langle XY | \eta_{32} | Z \rangle_{v_1} = -\frac{3}{2} \frac{\tilde{D}_{3;68}}{\sqrt{5}}, \quad (\text{C11})$$

$${}_g\langle XY | \eta_{31} | Z \rangle_{v_2} = 0, \quad (\text{C12})$$

$${}_g\langle XY | \eta_{32} | Z \rangle_{v_2} = -\frac{1}{2} \frac{\tilde{D}_{3;68}}{\sqrt{2}}, \quad (\text{C13})$$

In this case, the choice of our intermediate states spares us from a separate evaluation of the η_{31} component. The transition probability for the phonon assisted transition into the yellow series is then given by

$$P_{0,y} \propto |{}_y\langle XY | \eta_{32} | Z \rangle_b \langle Z | \mathbf{p} | 0 \rangle|^2 = \frac{1}{3} \tilde{D}_{3;68}^2 p_{35}^2, \quad (\text{C14})$$

the transition probability into the green series results in

$$P_{0,g} \propto \left| \sum_{i=1}^2 {}_g\langle XY | \eta_{32} | Z \rangle_{v_i} \langle Z | \mathbf{p} | 0 \rangle \right|^2 = \frac{2}{3} \tilde{D}_{3;68}^2 p_{35}^2. \quad (\text{C15})$$

From this we concur, that the ratio between yellow and green Γ_3^- phonon-assisted absorption has to be

$$\alpha_g^{\Gamma_3^-} : \alpha_y^{\Gamma_3^-} = 2 : 1. \quad (\text{C16})$$

¹ R. J. Elliott, Phys. Rev. **108**, 1384 (1957).

² N. Naka, S. Hashimoto, and T. Ishihara, Japanese Journal of Applied Physics **44**, 5096 (2005).

³ T. Kazimierczuk, D. Fröhlich, S. Scheel, H. Stolz, and M. Bayer, Nature **514**, 343 (2014).

⁴ P. Grünwald, M. Aßmann, J. Heckötter, D. Fröhlich, M. Bayer, H. Stolz, and S. Scheel, Phys. Rev. Lett. **117**, 133003 (2016).

⁵ J. Thewes, J. Heckötter, T. Kazimierczuk, M. Aßmann, D. Fröhlich, M. Bayer, M. A. Semina, and M. M. Glazov, Phys. Rev. Lett. **115**, 027402 (2015).

⁶ F. Schweiner, J. Main, and G. Wunner, Phys. Rev. B **93**, 085203 (2016).

⁷ J. Heckötter, M. Freitag, D. Fröhlich, M. Aßmann, M. Bayer, M. A. Semina, and M. M. Glazov, Phys. Rev. B **95**, 035210 (2017).

⁸ S. Zielińska-Raczyńska, D. Ziemkiewicz, and G. Czajkowski, Phys. Rev. B **94**, 045205 (2016).

⁹ F. Schöne, S.-O. Krüger, P. Grünwald, H. Stolz, S. Scheel, M. Aßmann, J. Heckötter, J. Thewes, D. Fröhlich, and M. Bayer, Phys. Rev. B **93**, 075203 (2016).

¹⁰ F. Schweiner, J. Main, and G. Wunner, Phys. Rev. Lett. **118**, 046401 (2017).

¹¹ Y. Toyozawa, Progress of Theoretical Physics **20**, 53 (1958).

¹² C. G. Kuper, Physics Today **16**, 106 (1963).

¹³ C. Malerba, F. Biccari, C. L. Ricardo, M. Dincau, P. Scardi, and A. Mittiga, Solar Energy Materials and Solar Cells **95**, 2848 (2011).

¹⁴ J. Robertson, Phys. Rev. B **28**, 3378 (1983).

¹⁵ P. Dawson, M. Hargreave, and G. Wilkinson, Journal of Physics and Chemistry of Solids **34**, 2201 (1973).

- ¹⁶ G. F. Koster, *Properties of the thirty-two point groups*, Vol. 24 (The MIT Press, 1963).
- ¹⁷ The scalar potential of the LO interaction does not modify the Bloch functions, hence can be extracted from the transition matrix elements.
- ¹⁸ P. Y. Yu and Y. R. Shen, Phys. Rev. B **12**, 1377 (1975).
- ¹⁹ R. Szmytkowski, Annalen der Physik **524**, 345 (2012).
- ²⁰ Ref.², copyright 2005 The Japan Society of Applied Physics.
- ²¹ The change in refractive index from 2.95 at the band edge to about 3.15³⁷ at the green excitons would give a correction of 2%, which is of order of the experimental error.
- ²² The consideration of the “spinless” symmetries is sufficient here. The spin-including symmetries open up additional transitory channels, however those require a change in the spin configuration, which cannot be inflicted by phonons.
- ²³ L. Kleinman and K. Mednick, Phys. Rev. B **21**, 1549 (1980).
- ²⁴ P. A. Korzhavyi and B. Johansson, *Literature review on the properties of cuprous oxide Cu₂O and the process of copper oxidation* (Swedish Nuclear Fuel and Waste Management Company, 2011).
- ²⁵ J. Brandt, D. Fröhlich, C. Sandfort, M. Bayer, H. Stolz, and N. Naka, Phys. Rev. Lett. **99**, 217403 (2007).
- ²⁶ F. Schweiner, J. Main, G. Wunner, and C. Uihlein, Phys. Rev. B **95**, 195201 (2017).
- ²⁷ C. Uihlein, D. Fröhlich, and R. Kenklies, Phys. Rev. B **23**, 2731 (1981).
- ²⁸ A. Daunois, J. L. Deiss, and B. Meyer, J. Phys. France **27** (1966), 10.1051/jphys:01966002703-4014200.
- ²⁹ P. Y. Yu and Y. R. Shen, Phys. Rev. B **17**, 4017 (1978).
- ³⁰ G. M. Kavoulakis and G. Baym, Phys. Rev. B **54**, 16625 (1996).
- ³¹ J. Heckötter, M. Freitag, D. Fröhlich, M. Afmann, M. Bayer, P. Grünwald, F. Schöne, D. Semkat, H. Stolz, and S. Scheel, “Rydberg excitons in the presence of an ultralow-density electron-hole plasma,” Submitted to Phys. Rev. Lett.
- ³² N. Naka, I. Akimoto, M. Shirai, and K. Kan’no, Phys. Rev. B **85**, 035209 (2012).
- ³³ A. Baldereschi and N. C. Lipari, Phys. Rev. B **3**, 439 (1971).
- ³⁴ J. Schmutzler, D. Fröhlich, and M. Bayer, Phys. Rev. B **87**, 245202 (2013).
- ³⁵ K. Suzuki and J. C. Hensel, Phys. Rev. B **9**, 4184 (1974).
- ³⁶ The momentum subscript **Q** is dropped here, since it carries no relevance in these considerations.
- ³⁷ T. Ito, T. Kawashima, H. Yamaguchi, T. Masumi, and S. Adachi, Journal of the Physical Society of Japan **67**, 2125 (1998).